## PAPER

# A polyimide-pyrolyzed carbon waste approach for the scalable and controlled electrochemical preparation of size-tunable graphene†

Haoguang Huang, Li Peng,* Wenzhang Fang, [ID] Shengying Cai, Xingyuan Chu, Yingjun Liu, Weiwei Gao, [ID] Zhen Xu* and Chao Gao [ID] *

Carbon materials are widely used in numerous fields, thus changing our lives. With the increasing consumption of carbon-based products, the disposal of consequent wastes has become a challenge due to their inert nature, which is hard to degrade, burn, or melt. Here, a recyclable strategy is proposed to deal with the explosive growth of carbon wastes. Through a fast and clean electrochemical method, carbon wastes are converted into functional building blocks of high value, such as graphene and graphene quantum dots (GQDs). For typical polyimide-pyrolyzed carbon (PPC), we establish the relationship between the chemical structure of raw materials and the characteristics of graphene products, including size and yield. The size-tunable graphene ranging from 3 nm to tens of micrometers is prepared by tuning the $sp^3/sp^2$ carbon ratio of PPC from 0.5 to 0 at adjustable temperatures (800 °C–2800 °C). Significantly, PPC with a bicontinuous structure (comprising $sp^2$ and $sp^3$) was efficiently cut into GQDs in 2 h with a high yield of 98%. Our protocol offers great potential for the scale-up preparations and applications of GQDs. Besides, we demonstrate that the GQDs performed well as dispersants to disperse hydrophobic carbon nanotubes (0.6 mg mL$^{-1}$) in water and improved the gravimetric capacitance of graphene-based supercapacitors by 79.4% with 3% GQDs added as nano-fillers.

## Introduction

Carbon materials have an unprecedented impact on modern industry and daily life, particularly in aerospace,[1] smart electronics,[2] energy fields,[3] and sports products, due to their excellent thermal, electrical, mechanical, and lightweight properties.[4–6] With the widespread applications of carbon products, the Carbon Age is likely coming after the Stone, Bronze, Iron and present Silicon Ages.[7] Nowadays, the demands towards artificial carbon materials, such as graphite papers and carbon fibers, are still growing.[8] Artificial carbon materials bring convenience to our life. However, the influence of carbon wastes on the environments and ecosystems would be intractable in the future, apart from the severe problem of microplastic waste.[9] More seriously, compared with exhaust gas and outlet water, the disposal of solid-state carbon materials is more difficult

MOE Key Laboratory of Macromolecular Synthesis and Functionalization, Department of Polymer Science and Engineering, Key Laboratory of Adsorption and Separation Materials & Technologies of Zhejiang Province, Zhejiang University, 38 Zheda Road, Hangzhou 310027, P. R. China. E-mail: sspengli@yeah.net, zhenxu@zju.edu.cn, chaogao@zju.edu.cn
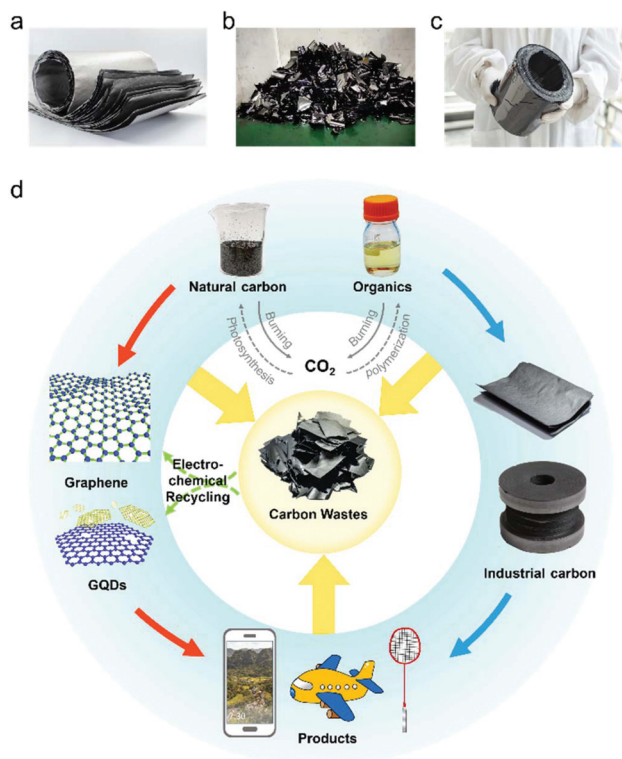†Electronic supplementary information (ESI) available. See DOI: 10.1039/d0nr00725k

because they are hard to degrade, burn, or melt.[10] Therefore, an effective recycling strategy to treat incremental carbon wastes (Fig. 1a–c) is of extreme significance.

Converting bulky wastes into low-dimensional carbon nano-materials opens an industrially viable avenue to conquer such a challenge. In particular, their carbonizable and graphitizable features make these wastes eligible as precursors for multi-functional graphene and GQDs.[10–12]

Regarding GQDs with a diameter smaller than 10 nm, the yield is always low when they are obtained from traditional precursors (*i.e.*, graphite,[13] graphenes,[14] graphene oxide,[15] carbon fibers,[16] carbon nanotubes,[17] and coal[18]) *via* chemical or electrochemical cutting methods.[17–20] The electrochemical strategy seems to be a better option for preparing GQDs, but it is difficult to achieve high-efficiency carbon conversion from these precursors. A large proportion of researchers devoted to changing the oxidant or other reaction conditions (*e.g.*, type or concentration of the electrolyte and electric current density) to achieve high conversion. However, the conversion is still relatively low (normally < 50%). Alternatively, the structure of precursors is probably critical for the carbon conversion of GQDs. The low-defect precursors (*i.e.*, graphite and carbon fiber) are more difficult to be etched into nanoscale products. For high-defect precursors (*i.e.*, reduced graphene oxide and coal), their

**Fig. 1** (a) Industrial PPC graphite paper and (b) the corresponding wastes produced during their manufacturing process. (c) The coiled material select from b. (d) Carbon cycle diagram.

porous or layered structure is prone to be split by electrolytic bubbles ($O_2$, $H_2$), producing plenty of non-electrolyzed sediments rather than GQDs.[14–20]

Here, we present a recycling strategy to convert the polyimide-pyrolyzed industrial carbon wastes into size-tunable graphene products with high value *via* a clean electrochemical method. The controllable $sp^3/sp^2$ C ratio ($C_r$) of polyimide-pyrolyzed carbon (PPC) determines the size and yield of nano-scale GQDs and micron-sized graphene sheets. Significantly, the precursors with a bicontinuous structure ($sp^2$ and $sp^3$ C) can avoid the breakage caused by electrolytic bubbling effect, realizing a high carbon conversion (77.4%) and yield (98%) of GQDs within 2 h. The functionalized GQDs are demonstrated to be a good surfactant for dispersing carbon nanotubes with a high dispersion concentration of 0.6 mg mL$^{-1}$. In addition, GQDs are used to be the accessory ingredients for high-performance supercapacitors. The macroscopic assembly graphene materials with 3% GQDs can realize a 79.4% improvement in the gravimetric capacitance. This study not only offers a new insight to dispose industrial wastes but also opens an avenue to a high-efficiency and selective preparation of graphene materials.

## Results and discussion

As shown in Fig. 1d, a recycling strategy is provided to deal with the ceaselessly produced carbon wastes. Through a clean

electrochemical method, the graphene ($C_r \leq 0.08$) or GQDs ($C_r \geq 0.08$) are prepared by selecting carbon wastes with controlled $C_r$ (Fig. S1 and Table S1†). Therefore, the products can become the building blocks of other functional materials to take part in the carbon cycle again.

The yields of GQDs are relatively low when using precursors with layered or polyporous structures (graphene,[14] carbon nanotube,[17] coal,[18] and carbon fiber[16]), even if they have more $sp^3$ C.[21–23] Non-negligible fracture and exfoliation are induced by the bubbling effect of the electrolytic gas ($O_2$, $H_2$). Then, the departed debris from the electrodes drops in the electrolyte and cannot hold a subsequent reaction. To resolve the problems posed by the conventional precursors, it is necessary to choose an alternative carbon electrode with the bicontinuous structure of $sp^3$ C and $sp^2$ C. Considering that the carbon matrix with less $sp^3$ C can reduce the C loss during the preparation process, lower $C_r$ is also important. Although the conventional precursors have gained widespread use in the preparation of GQDs,[14–18] their structure is difficult to adjust. Therefore, conventional precursors are not suitable research objects in this study. After numerous analyses, we identified graphitizable polymers, particularly the widely used pitch, carbon fibers, and PPC graphitic papers in industries, as an alternative choice.[24–26] In contrast to non-graphitizable polymers, the graphitizable ones have a higher carbonization degree, which can reduce the loss of $sp^3$ C and improve the yield. In this study, the 800–2800 °C-treated PPC films (named as PPC-X, X denotes the treatment temperature) are used as the typical carbon electrodes.

Fig. 2a shows the preparation process of GQDs. Typically, 0.8 g PPC-1300 was selected as the anode. Since weak electrolytes have demonstrated a good cutting effect in the preparation of GQDs,[14] a dilute ammonia solution (800 mL, 0.05 mol L$^{-1}$) was used as the electrolyte. The electrochemical reaction was completed in 2 h at room temperature with the color of the electrolyte changing from transparent to black. The concentration of the GQDs is 0.75 mg mL$^{-1}$ (the detailed calculation method is shown in the ESI†). After the volatilization of ammonia,[14,15] the purified GQDs were obtained (Fig. 2b). The concentration of the as-prepared GQDs can be regulated by evaporating redundant water at 60 °C with the highest value up to 82 mg mL$^{-1}$ (Fig. 2c). The highly concentrated solution benefits for the storage and transportation of GQDs. Fig. 2d illustrates the Chinese calligraphy written using GQD inks with a concentration of 52 mg mL$^{-1}$. We evaluate the quantum yield (QY) changes of GQDs with different concentrations.[27,28] Interestingly, the solid-state fluorescence quenching emerges with the aggregation of GQDs, but QY does not show evident fluctuation when the GQDs are dissolved in the water again (Fig. 2e). For the accurate analysis of yield, we give methods to calculate the yield and carbon conversion rate. As shown in Fig. 2f, the yield and carbon conversion of this method are 98% and 77.4%, respectively. The values are both higher than those previously reported.
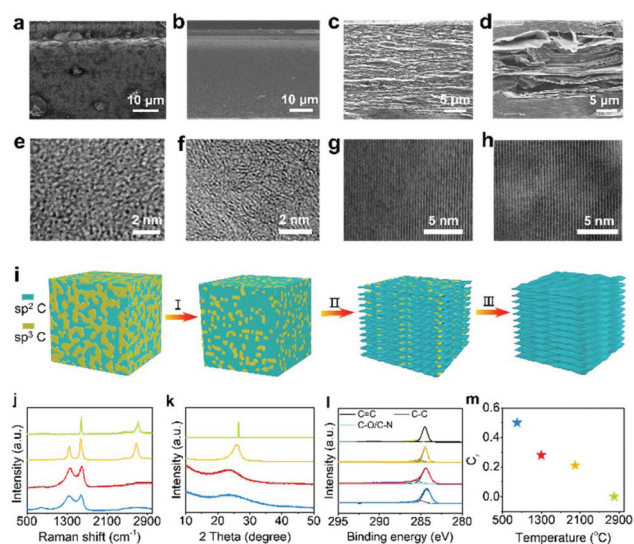
To gain insight into the extremely high yield of the GQDs obtained from PPC-1300, the structure evolution of PPC with
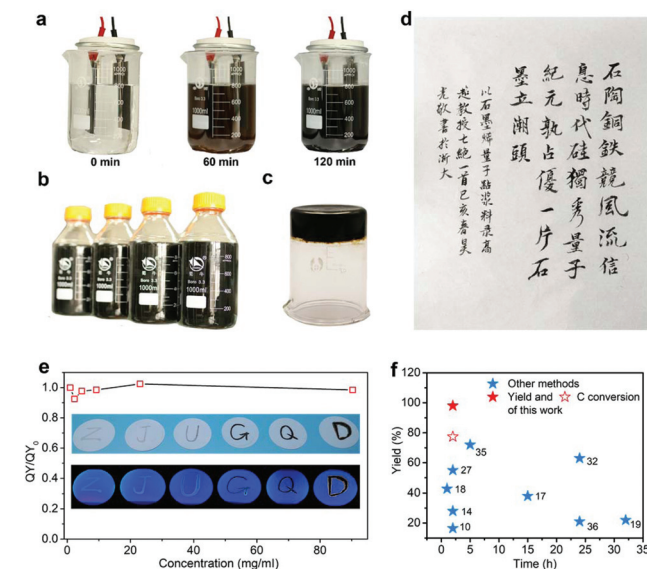
**Fig. 2** (a) The electrochemical preparation process of GQDs. (b) Mass-produced GQD aqueous solution with a concentration of 2 mg ml$^{-1}$. (c) High concentration (79 mg ml$^{-1}$) of the GQD aqueous solution. (d) The Chinese calligraphy written with GQD ink having a concentration of 52 mg ml$^{-1}$. (e) QY changes with the concentration of the GQDs. Inset: letters of Z, J, U, G, Q, D written by GQD inks with a concentration of 0.92, 2.3, 4.6, 9.2, 23, 90.3 mg ml$^{-1}$. (f) A summary of the yield and carbon conversion of GQDs fabricated in this study and yields obtained by other methods.



**Fig. 3** (a–d) SEM image of the edge of fractured PPC-800, PPC-1300, PPC-2000 and PPC-2800. (e–h) HRTEM image of the surface of PPC-800, PPC-1300, PPC-2000, and PPC-2800. (i) The corresponding models of PPC based on (a–h). (j) Raman spectra, (k) XRD, (l) XPS surveys and (m) $C_r$ of PPC-800 (blue mark), PPC-1300 (red mark), PPC-2000 (orange mark) and PPC-2800 (green mark), respectively.

annealing temperatures was characterized using scanning electron microscopy (SEM).[25,26] As shown in Fig. 3a–d, the PPC-800 presents a polyporous morphology, which was not found in the fractured surface of PPC-1300. When the temperature reaches 2000 °C, the PPC film shows an evident laminated structure. It can be concluded that the PPC undergoes an isotropic densification process at 800–1300 °C and then tend to form an oriented layered structure after 1300 °C annealing. To further investigate the structure evolution, high-resolution transmission electron microscopy (HRTEM, Fig. 3e–h) was performed to characterize the microstructures of PPC. The randomly-fractured surfaces of PPC-800 and PPC-1300 exhibited a bicontinuous structure of sp$^2$ and sp$^3$ C. When the temperature exceeds 2000 °C, a highly oriented layered structure is seen on the cross-section of the PPC film.[29,30] These results illustrate that the bicontinuous structure is an important factor for the high yield preparation of GQDs, and therefore the highest yield can be achieved from PPC-1300.

The visual models simulate the three stages of the structure evolution for PPC films, including the bicontinuous stage (800–1300 °C), the evolution of the laminated structure (1300–2000 °C), and repair of sp$^3$ C (2000–2800 °C). In the first stage, the bicontinuous structure is maintained and the lattice size grows with the increase in temperature from 800 to 1300 °C (Fig. S2†). In the second stage, the layered structure is formed, oriented at the in-plane direction of the film. In the third stage, the sp$^3$ C in the layered PPC films converts into sp$^2$ C and forms a typical sea-island structure (Fig. 3i). From

the changed structure of the PPC films, it is speculated that the PPC films are suitable for the preparation of GQDs when treated at 800–2000 °C and the fabrication of graphene occurs after 2000–2800 °C thermal annealing.

Raman spectroscopy, X-ray powder diffraction (XRD) and X-ray photoelectron spectroscopy (XPS) were performed to investigate the chemical structure evolution of these PPC films. In the first stage, both PPC-800 and PPC-1300 showed abundant defects (sp$^3$ C) with the high $I_D/I_G$ values of 0.96 and 0.91, respectively (Fig. 3j). In the XRD patterns of PPC-800 and PPC-1300, the broad peaks around 23.3° and 42.8° correspond to the diffraction of the (002) and (100) planes, which indicates a highly disordered carbon structure. The (100) peak sharpens with the carbonization temperature, increasing from 800 °C to 1300 °C, which demonstrates the gradually ordered arrangement in the PPC film (Fig. S3†).[30] In the second stage, the Raman spectra show an increase in sp$^2$ C with $I_D/I_G$ decreasing from 0.91 to 0.62 and a shift in the G peak from 1590.4 cm$^{-1}$ to 1577.3 cm$^{-1}$. The emerged 2D peak suggests the generation of the layered structure after high-temperature annealing,[23,31] which is confirmed by the narrowed half peak width of $2\theta$ (Fig. 3k). In the third stage, the D peak in the Raman spectrum disappears, and the $2\theta$ peak of the XRD pattern becomes very sharp. These results indicate a progressive graphitization of PPC films with temperature from 2000 °C to 2800 °C.[23] The XPS survey exhibits the adjustable element contents and compositions with temperature. The amount of carbon increases from 93.6% to 98.3%, oxygen decreases from 3.1% to 1.7%, and nitrogen reduces from 3.3% to 0 during the whole annealing process (Table S2†). The corresponding $C_r$ values of PPC-800 (Fig. 3l and m), PPC-1300, PPC-2000 and PPC-2800

calculated based on C 1 s spectra are 0.5, 0.28, 0.21, and 0, respectively.[32,33]

Given these results, the graphitizable polymers (such as polyimide) with the bicontinuous structure have few holes and oriented layers that are ubiquitous in traditional precursors. Therefore, the breakage problems caused by electrolytic bubbling ($O_2$, $H_2$) effect within the structural defects are solved. Compared with the other materials, PPC-1300 with the bicontinuous structure possesses a lower $C_r$ and hence achieves a high yield (98%). Besides, the yield decreases during the transformation process from the bicontinuous structure to the layered structure. However, a high level of yield is still maintained because of the existence of the bicontinuous structure. For example, the yield of PPC-1600 is 74%.

The size of GQDs has a positive correlation with the $C_r$ of the anode materials. The morphology and average lateral size of GQDs were characterized via TEM (Fig. 4a–d and S4–7†). The measured sizes of GQDs-800, GQDs-1300, GQDs-1600 and GQDs-2000 are 3.9 nm, 4.76 nm, 5.95 nm and 7.45 nm, respectively (GQDs-X is prepared by PPC-X, Fig. 4e–h).[23] The fluorescence of GQDs shows red-shift along with the increase in the size (Fig. S8 and 9†). The GQDs show a high crystallinity with a lattice space of 0.21 nm, corresponding to the hexagonal lattice plane spacing of $d_{1100}$ (Fig. S10†).[33,34] The AFM image indicates that the thickness of the GQDs is within 1–6 atom layers (Fig. S11†). Besides, the chemical structures of these GQDs also have been investigated via Raman spectroscopy and XPS, which are consistent with those for the samples prepared by other methods (Fig. S12–14†).[35–37]

The PPC with $C_r \leq 0.08$ (2300–2800 °C) is a suitable anode for fabricating graphene in high yields (Fig. S15†). The cut process rarely occurs on the anode because few sp$^3$ C are contained in the PPC at this stage. Besides, the isotropic PPC

film evolves to oriented film along the in-plane direction and the layered structure is shown (Fig. 3e–h). The highly oriented layered structure facilitates the ion intercalation during the electrochemical exfoliation process, forming micron-sized graphene. To confirm this, the PPC-X (X ranges from 2300 °C to 2800 °C) is used as an anode for electrochemical reactions in the diluted ammonium sulfate solution (1 mol L$^{-1}$, $(NH_4)_2SO_4$).[38,39] Fig. 4i illustrates the flexible graphene sheets with network ripples exfoliated from PPC-2800. The few-layered structure of the obtained graphene is shown in Fig. 4j.

Fig. 4k summarizes the influence of $C_r$ on the size and yield of the product. The size shows a regular growth with a decrease in the $C_r$ value from 0.5 to 0. The yield is affected by the structural transformation of PPC during the heating process. During the bicontinuous stage of the structural evolution of PPC films, the materials with low $C_r$ will cut the loss of sp$^3$ C in the electrochemical cutting process, improving the carbon conversion and the yield of the product. However, an inverse tendency is presented when annealing temperature surpasses 1300 °C. Compared to PPC-1300, PPC-1600 has a similar $C_r$ but a relatively low yield of 74%, ascribing to the formation of the laminated structure (Fig. S16†). These results illustrate that the bicontinuous structure and low $C_r$ are both critical for preparing GQDs with a high yield. Notably, using PPC-2300 as the precursor, an ultralow preparation yield (<1%) of GQDs is obtained, whereas the high yield (82%) is achieved when it is used to fabricate graphene. These results suggest that the highly-restored PPC is not the preferred precursor for the fabrication of GQDs but is a good choice for the preparation of micron-sized graphene.

Benefiting from the high yield and mass preparation, the GQDs can satisfy gram-scale demands. It is known that GQDs possess excellent aqueous dispersion stability owing to their nano-size and hydrophilic groups, which are superior to the micron-sized graphene oxide with a single layer.[40] As shown in Fig. 5a, the hydrophobic multi-walled carbon nanotubes (CNTs) dispersed with the GQDs exhibit good dispersion stability with an average zeta potential of −37.1 mV. The TEM image shows that the GQDs are uniformly distributed around the CNTs (Fig. 5b). Therefore, the GQDs fabricated by this low-cost method are eligible for the dispersion of hydrophobic carbon materials in the industry.

Many efforts have been devoted to enhancing the electronic properties of graphene supercapacitors by doping heteroatoms in graphene, but the doping process is difficult to achieve. The GQDs-1300 presents a large specific surface area and plentiful N doping. Thus, we introduce the GQDs into GO aerogel supercapacitors (X-GQDs/GOCs, X is the proportion of GQDs in the mixture) to meet this challenge. As shown in Fig. 5c and S17,† the cyclic voltammetry (CV) curve of the GO supercapacitor (GOCs) displays a rectangular shape, reflecting the typical electric double-layer capacitor (EDLC) behavior. In contrast, the GQDs/GOCs exhibit a nonrectangular shape with faradaic redox peaks in the potential range of 0–0.5 V, suggesting an accessional pseudocapacitive apart from
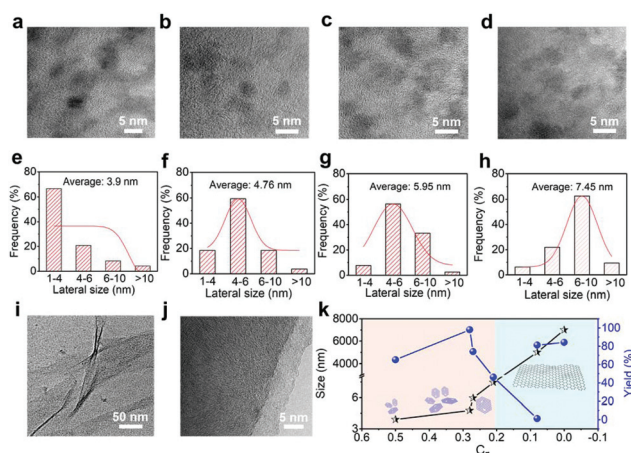


Fig. 4 (a–d) TEM images and (e–h) corresponding size distribution histograms with the Gaussian fitting curve of the GQDs fabricated by PPC-800, PPC-1300, PPC-1600, and PPC-2000, respectively. The sizes are counted based on Fig. 4a–d and Fig. S3–6.† (i) TEM image of a wrinkled graphene sheet. (j) HRTEM. (k) A summary diagram for the influence of size and yield by $C_r$.
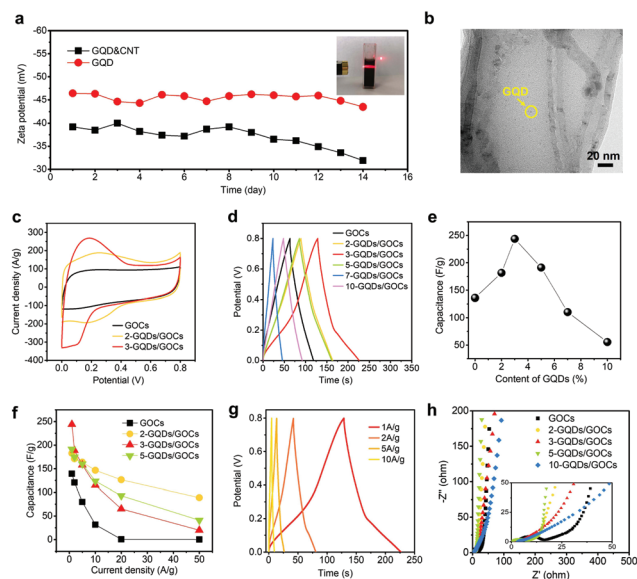
Fig. 5 (a) Zeta potential changes of GQDs and GQD&CNT with time. (b) TEM image of GQDs dispersed CNTs. (c) CV tests of GOCs, 2-GQDs/GOCs and 3-GQDs/GOCs at 10 mV s⁻¹. (d) GCD tests. (e) $C_s$ changes of GO with the addion of GQDs. (f) Rate performance while current density increased from 0.1 A g⁻¹ to 50 A g⁻¹. (g) GCD curves for 3-GQDs/GOCs at different current densities from 1 to 10 A g⁻¹. (h) EIS test.

size and yield was obtained. The precursors with a bicontinuous (sp$^2$ and sp$^3$ C) structure obtained from graphitizable polymers could elevate the yield of GQDs. The PPC-1300 achieved the highest yield of 98% at a carbon conversion of 77.4%. This high efficient procedure of GQD production opens a new avenue for GQDs to realize their applications in industrial products, such as dispersant and functional filler. The hydrophobic CNTs (0.6 mg mL⁻¹) show stable dispersibility with the assistant of the small-sized and amphiphilic GQDs. Besides, a 79.4% improvement in the gravimetric capacitance of the GO supercapacitor was achieved by adding 3% N-doped GQDs. Through this recyclable strategy, we give a foresight for the disposal of industrial carbon wastes and propose the structure selection law by connecting the structure of precursors with anticipant products.

EDLC (Fig. S18†).[41] The gravimetric capacitance ($C_s$) is calculated from galvanostatic charge/discharge curves (GCD). Significantly, the ratio of GQDs/GO affects the electrochemical performance of the supercapacitors (Fig. 5d). The introduction of GQDs enhances the gravimetric capacitance ($C_s$). The highest $C_s$ of 244 F g⁻¹ is achieved with GQD contents of 3%, showing a 79.4% enhancement than that of pure GO supercapacitors. Subsequently, the $C_s$ gradually decreases with the continuous addition of GQDs (Fig. 5e). This is because excess GQDs reduce the conductivity of the supercapacitors.[3] Moreover, the rate performance of GQDs/GOCs is superior to GOCs (Fig. 5f and S19 and 20†). The capacitance retentions of 2-GQDs/GOCs and 3-GQDs/GOCs are 125.5 F g⁻¹ and 65 F g⁻¹ from 1 to 20 A g⁻¹, whereas the value of GOCs becomes zero (Fig. 5g). The equivalent series resistance ($R_{ESR}$) based on the Nyquist plots was determined.[42] The $R_{ESR}$ of 2-GQDs/GOCs and 3-GQDs/GOCs are 2.7 Ω and 4.8 Ω, respectively (Fig. 5h). These values are much lower than that of GOCs (13.1 Ω), suggesting that the rapid ion diffusion channel and short diffusion distance are provided by GQDs.[43]

## Conclusions

In summary, a recycling strategy was established to convert the polyimide-pyrolyzed industrial carbon wastes into size-tunable graphene *via* a simple and clean electrochemical method. The relationship between the chemical structure of the carbon anode and characteristics of the graphene products including

## Experimental

### Materials

All the reagents were of analytical grade and used as received. Graphene oxide (GO) with an average lateral size of 5 μm was bought from GaoxiTech Co. Ltd (http://www.gaoxitech.com/). PPC was provided by Guangdong Suqun New Materials CO. Ltd.

### Fabrication of GQDs

GQDs were fabricated *via* a water-phase strategy, which was a one-step electrochemical process. Typically, 0.4 g PPC-X (X = 800, 1300, 1600, 2000) was used as the working electrode and a high-pressure graphite plate electrode (100 mm × 60 mm) was used as the cathode. 800 ml, 0.05 mol L⁻¹ NH₃·H₂O was used as the electrolyte. The constant distance between the anode and cathode was ∼2 cm in the electrochemical process. The electrochemical exfoliation was carried out by applying a positive voltage (3–30 V) to the anode at 25 °C through a UNI-T UTP3305 DC power within 2 h. The large non-luminescent fraction was removed by vacuum filtration. A filter membrane with a pore size of 100 nm was used. Then, the purified GQDs were obtained after ammonia volatilization. The concentrated GQD inks were obtained by evaporating water at 60 °C. The QY of GQDs could be enhanced *via* an 80 °C hydrothermal treatment in the H₂O₂ solution.

### Preparation of graphene

Graphene was fabricated *via* one-step electrochemistry combined with an ultrasound process. Typically, a graphite foil (50 mm × 10 mm × 0.5 mm) was used as the working electrode and a platinum (Pt) flake electrode (50 mm × 10 mm) as the cathode. The electrolyte was prepared by dissolving 13.2 g (NH₄)₂SO₄ in 100 mL of deionized H₂O with a concentration of 1 M. The constant distance between the anode and cathode was ∼2 cm in the electrochemical process. The electrochemical exfoliation was carried out by applying a positive voltage (5 V) to the anode at 25 °C *via* a UNI-T UTP3305 DC power source. Then, the obtained materials were washed by deionized water

using vacuum filtration until the filtrate turned neutral. The purified products were dispersed in methyl pyrrolidone again to obtain few-layer graphene by the sonication process for 30 min, and centrifugation twice at 3000 rpm for 10 min to remove the thick graphene sheets.

### Preparation of aqueous dispersion of CNTs

The aqueous dispersion of CNTs was prepared using an ultrasonic water bath with simultaneous mechanical agitation. Typically, 200 mg of graphene was added to 250 mL of 0.25 mg mL$^{-1}$ GQD solution to realize the dispersion process in 2 h. The non-dispersed parts were removed by centrifugation at 3000 rpm. Then, the dispersion was filtrated through a PVDF membrane (Millipore, pore size: 100 nm) under continuous stirring to remove the redundant GQDs, followed by the redispersion of the residue with deionized water.

### Preparation of supercapacitors

The GOC foam was obtained by the freeze-drying of 10 g of 10 mg g$^{-1}$ GO slurry. X-GQDs/GOCs ($X$ = 1, 2, 3, 5, 7, and 10) was prepared by mixing the GQD solution with GO slurry in the calculative proportion. The X represents the percentage of GQDs in the mixture. The foam of the X-GQDs/GOCs also fabricated through the freeze-drying process. Then, the GOCs and X-GQDs/GOCs were immersed in the hydriodic acid ethanol/water (3 : 1 v/v) solution for 2 h at 90 °C for reduction, followed by ethanol washing repeatedly. The obtained materials were further dipped in 1 mol L$^{-1}$ H$_2$SO$_4$ for 4 h for the electrochemical tests.

### Characterization

Scanning electron microscopy (SEM) images were taken on a Hitachi S4800 field emission system. Transmission electron microscopy (TEM) characterizations were carried out on a Titan ChemiS TEM (FEI) instrument with a probe correction apparatus and a JEM 2100F. The AFM image was taken in the tapping mode on a NanoScope IIIA. Raman spectra were recorded on a Renishaw inVia-Reflex Raman microscope using a 532 nm laser source. The crystallite dimensions (La) were determined using the empirical formula: La (nm) = $(2.4 \times 10^{-10})$ $\lambda^4$ $(I_D/I_G)^{-1}$, where the $\lambda$ is the laser wavelength and $(I_D/I_G)$ is the integrated intensity ratio of the D band and G band. XPS was performed using the Thermo ESCALAB 250Xi spectrometer. XRD data were collected on an X'Pert Pro (PANalytical) diffractometer using monochromatic Cu Kα1 radiation ($\lambda$ = 1.5406 Å) at 40 kV. Fourier transform infrared spectra were recorded on a PE Paragon 1000 spectrometer (film or KBr disk). The photoluminescence (PL) spectra were measured using a QM-40 spectrofluorometer (PTI, Horiba) equipped with a 150 W xenon lamp. The transient photoluminescence decay was collected by the TCSPC technique. Ultraviolet–visible spectra were obtained using a Varian Cary 300 Bio instrument. Zeta potentials were measured on a Zetasizer Nano-ZS instrument. CV, EIS, and GCD measurements were performed using an electrochemical workstation (CHI660e, CH Instruments, Inc.).

## Conflicts of interest

There are no conflicts to declare.

## Acknowledgements

## Notes and references

1 D. Choi, H. Kil and S. Lee, Fabrication of Low-Cost Carbon Fibers Using Economical Precursors and Advanced Processing Technologies, *Carbon*, 2019, **142**, 610–649.

2 Y. Ding, H. Hou, Y. Zhao, Z. Zhu and H. Fong, Electrospun Polyimide Nanofibers and Their Applications, *Prog. Polym. Sci.*, 2016, **61**, 67–103.

3 S. Cai, T. Huang, H. Chen, M. Salman, K. Gopalsamy and C. Gao, Wet-Spinning of Ternary Synergistic Coaxial Fibers for High Performance Yarn Supercapacitors, *J. Mater. Chem. A*, 2017, **5**, 22489.

4 Y. Wen, M. Wu, M. Zhang, C. Li and G. Shi, Topological Design of Ultrastrong and Highly Conductive Graphene Films, *Adv. Mater.*, 2017, **29**, 1702831.

5 I. Kinloch, J. Suhr, J. Lou, R. Young and P. Ajayan, Composites with carbon nanotubes and graphene: An outlook, *Science*, 2018, **362**, 547–553.

6 T. Booth, P. Blake, R. Nair, D. Jiang, E. Hill, U. Bangert, A. Bleloch, M. Gass, K. Novoselov, M. Katsnelson and A. Geim, Macroscopic Graphene Membranes and Their Extraordinary Stiffness, *Nano Lett.*, 2008, **8**, 2442–2446.

7 H. Brody, Graphene, *Nature*, 2012, **483**, S29.

8 J. Deng, Y. You, V. Sahajwalla and R. Joshi, Transforming waste into carbon-based nanomaterials, *Carbon*, 2016, **96**, 105–115.

9 M. Shen, Y. Zhu, Y. Zhang, G. Zeng, X. Wen, H. Yi, S. Ye, X. Ren and B. Song, Micro(nano)plastics: Unignorable Vectors for Organisms, *Mar. Pollut. Bull.*, 2019, **139**, 28–33.

10 H. Ming, Z. Ma, Y. Liu, K. Pan, H. Yu, F. Wang and Z. Kang, Large scale electrochemical synthesis of high quality carbon nanodots and their photocatalytic property, *Dalton Trans.*, 2012, **41**, 9526–9531.

11 X. Miao, D. Qu, D. Yang, B. Nie, Y. Zhao, H. Fan and Z. Sun, Synthesis of Carbon Dots with Multiple Color

Emission by Controlled Graphitization and Surface Functionalization, *Adv. Mater.*, 2018, **30**, 1704740.

12 H. Ding, S. Yu, J. Wei and H. Xiong, Full-Color Light-Emitting Carbon Dots with a Surface-State-Controlled Luminescence Mechanism, *ACS Nano*, 2016, **10**, 484–491.

13 X. Tan, Y. Li, X. Li, S. Zhou, L. Fan and S. Yang, Electrochemical Synthesis of Small-Sized Red Fluorescent Graphene Quantum Dots as a Bioimaging Platform, *Chem. Commun.*, 2015, **51**, 2544–2546.

14 H. Huang, S. Yang, Q. Li, Y. Yang, G. Wang, X. You, B. Mao, H. Wang, Y. Ma, P. He, Z. Liu, G. Ding and X. Xie, Electrochemical Cutting in Weak Aqueous Electrolytes: The Strategy for Efficient and Controllable Preparation of Graphene Quantum Dots, *Langmuir*, 2018, **34**, 250–258.

15 H. Tetsuka, R. Asahi, A. Nagoya, K. Okamoto, I. Tajima, R. Ohta and A. Okamoto, Optically Tunable Amino-Functionalized Graphene Quantum Dots, *Adv. Mater.*, 2012, **24**, 5333–5338.

16 J. Peng, W. Gao, B. Gupta, Z. Liu, R. Romero-Aburto, L. Ge, L. Song, L. Alemany, X. Zhan, G. Gao, S. Vithayathil, B. Kaipparettu, A. Marti, T. Hayashi, J. Zhu and P. Ajayan, Graphene Quantum Dots Derived from Carbon Fibers, *Nano Lett.*, 2012, **12**, 844–849.

17 D. Shinde and V. Pillai, Electrochemical Preparation of Luminescent Graphene Quantum Dots from Multiwalled Carbon Nanotubes, *Chem. – Eur. J.*, 2012, **18**, 12522–12528.

18 M. He, X. Guo, J. Huang, H. Shen, Q. Zeng and L. Wang, Mass Production of Tunable Multicolor Graphene Quantum Dots from An Energy Resource of Coke by A One-Step Electrochemical Exfoliation, *Carbon*, 2018, **140**, 508–520.

19 D. Pan, J. Zhang, Z. Li and M. Wu, Hydrothermal Route for Cutting Graphene Sheets into Blue-Luminescent Graphene Quantum Dots, *Adv. Mater.*, 2010, **22**, 734–738.

20 A. Ananthanarayanan, X. Wang, P. Routh, B. Sana, S. Lim, D. Kim, K. Lim, J. Li and P. Chen, Facile Synthesis of Graphene Quantum Dots from 3D Graphene and their Application for Fe3+Sensing, *Adv. Funct. Mater.*, 2014, **24**, 3021–3026.

21 Y. Hishiyama, A. Yoshida, Y. Kaburagi and M. Inagaki, Graphite films prepared from carbonized polyimide films, *Carbon*, 1992, **30**, 333–337.

22 S. Yang, Y. Yang, P. He, G. Wang, G. Ding and X. Xie, Insights into the Oxidation Mechanism of Sp2−Sp3 Hybrid Carbon Materials: Preparation of a Water-Soluble 2D Porous Conductive Network and Detectable Molecule Separation, *Langmuir*, 2017, **33**, 913–919.

23 L. Peng, Z. Xu, Z. Liu, Y. Guo, P. Li and C. Gao, Ultrahigh Thermal Conductive yet Superflexible Graphene Films, *Adv. Mater.*, 2017, **29**, 1700589.

24 Y. Li, Y. Zhao, H. Cheng, Y. Hu, G. Shi, L. Dai and L. Qu, Nitrogen-Doped Graphene Quantum Dots with Oxygen-Rich Functional Groups, *J. Am. Chem. Soc.*, 2011, **134**, 15–18.

25 H. Hatori, Y. Yamada and M. Shiraishi, In-plane orientation and graphitizability of polyimide films, *Carbon*, 1992, **30**, 763–766.

26 M. Murakami, A. Tatami and M. Tachibana, Fabrication of high quality and large area graphite thin films by pyrolysis and graphitization of polyimides, *Carbon*, 2019, **145**, 23–30.

27 C. Wang, W. Wu, A. Periasamy and H. Chang, Electrochemical Synthesis of Photoluminescent Carbon Nanodots from Glycine for Highly Sensitive Detection of Hemoglobin, *Green Chem.*, 2014, **16**, 2509–2514.

28 Y. Choi, B. Kang, J. Lee, S. Kim, G. Kim, H. Kang, B. Lee, H. Kim, S. Shim, G. Lee, O. Kwon and B. Kim, Integrative Approach toward Uncovering the Origin of Photoluminescence in Dual Heteroatom-Doped Carbon Nanodots, *Chem. Mater.*, 2016, **28**, 6840–6847.

29 Q. Wei, S. Pei, G. Wen, K. Huang, Z. Wu, Z. Liu, W. Ma, H. Cheng and W. Ren, High Yield Controlled Synthesis of Nano-Graphene Oxide by Water Electrolytic Oxidation of Glassy Carbon for Metal-Free Catalysis, *ACS Nano*, 2019, **13**, 9482–9490.

30 S. Zhao, Z. Shi, C. Wang and M. Chen, Structure and Surface Elemental State Analysis of Polyimide Resin Film after Carbonization and Graphitization, *J. Appl. Polym. Sci.*, 2008, **108**, 1852–1856.

31 I. Jeon, B. Yoon, M. He and T. Swager, Hyperstage Graphite: Electrochemical Synthesis and Spontaneous Reactive Exfoliation, *Adv. Mater.*, 2018, **30**, 1704538.

32 L. Wang, Y. Wang, T. Xu, H. Liao, C. Yao, Y. Liu, Z. Li, Z. Chen, D. Pan, L. Sun and M. Wu, Gram-Scale Synthesis of Single-Crystalline Graphene Quantum Dots with Superior Optical Properties, *Nat. Commun.*, 2014, **5**, 5357.

33 H. Ding, S. Yu, J. Wei and H. Xiong, Full-Color Light-Emitting Carbon Dots with a Surface-State-Controlled Luminescence Mechanism, *ACS Nano*, 2016, **10**, 484–491.

34 Y. Li, H. Liu, X. Liu, S. Li, L. Wang, N. Ma and D. Qiu, Free-Radical-Assisted Rapid Synthesis of Graphene Quantum Dots and Their Oxidizability Studies, *Langmuir*, 2016, **32**, 8641–8649.

35 H. v. Park, S. Noh, J. Lee, W. Lee, J. Jaung, S. Lee and T. Han, Large Scale Synthesis and Light Emitting Fibers of Tailor-Made Graphene Quantum Dots, *Sci. Rep.*, 2015, **5**, 14163.

36 R. Ye, C. Xiang, J. Lin, Z. Peng, K. Huang, Z. Yan, N. Cook, E. Samuel, C. Hwang, G. Ruan, G. Ceriotti, A. Raji, A. Martí and J. Tour, Coal as an abundant source of graphene quantum dots, *Nat. Commun.*, 2013, **4**, 2943–2948.

37 Z. Ding, F. Li, J. Wen, X. Wang and R. Sun, Gram-Scale Synthesis of Single-Crystalline Graphene Quantum Dots Derived From Lignin Biomass, *Green Chem.*, 2018, **20**, 1383–1390.

38 S. Pei, Q. Wei, K. Huang, H. Cheng and W. Ren, Green Synthesis of Graphene Oxide by Seconds Timescale Water Electrolytic Oxidation, *Nat. Commun.*, 2018, **9**, 145.

39 S. Yang, S. Brüller, Z. Wu, Z. Liu, K. Parvez, R. Dong, F. Richard, P. Samorì, X. Feng and K. Müllen, Organic Radical-Assisted Electrochemical Exfoliation for the Scalable Production of High-Quality Graphene, *J. Am. Chem. Soc.*, 2015, **137**, 13927–13932.

40 P. He, J. Sun, S. Tian, S. Yang, S. Ding, G. Ding, X. Xie and M. Jiang, Processable Aqueous Dispersions of Graphene

Stabilized by Graphene Quantum Dots, *Chem. Mater.*, 2015, **27**, 218–226.

41 Q. Li, H. Cheng, X. Wu, C. Wang, G. Wu and S. Chen, Enriched Carbon Dots/Graphene Microfibers Towards High-Performance Micro-Supercapacitors, *J. Mater. Chem. A*, 2018, **6**, 14112.

42 J. Zhao, Y. Jiang, H. Fan, M. Liu, O. Zhuo, X. Wang, Q. Wu, L. Yang, Y. Ma and Z. Hu, Porous 3D Few-Layer Graphene-like Carbon for Ultrahigh-Power Supercapacitors with Well-Defined Structure–Performance Relationship, *Adv. Mater.*, 2017, **29**, 1604569.

43 T. Huang, X. Chu, S. Cai, Q. Yang, H. Chen, Y. Liu, K. Gopalsamy, Z. Xu, W. Gao and C. Gao, Tri-High Designed Graphene Electrodes for Long Cycle-Life Supercapacitors with High Mass Loading, *Energy Storage Mater.*, 2019, **17**, 349–357.